JOURNAL OF ENERGY SYSTEMS

2022, 6(4)

2602-2052 DOI: 10.30521/jes.1105215 Research Article

The features of the InGaAs/InP detectors in plasma converter systems

Hatice Hilal Yücel (Kurt)
Gazi University, Faculty of Science, Department of Physics, 06500 Teknikokullar, Ankara, Türkiye, hkurt@gazi.edu.tr

Selçuk Utaş*
Gazi University, Faculty of Science, Department of Physics, 06500 Teknikokullar, Ankara, Türkiye, selcuk.utas@gmail.com

Submitted: 18.04.2022
Accepted: 01.11.2022
Published: 31.12.2022

* *Corresponding Author*

Abstract: The features of the plasma cell with the InGaAs/InP detector are explored. The detector is composed of InGaAs and InP wafers. Mean electron energies, migrative electron flux and current densities are evaluated by theoretical simulation analyses. The results helped to understand the uncertain plasma parameters and made the plasma structure more understandable, thereby, the complex plasma reactions can be solved via the COMSOL package. New plasma studies have focused on uniform discharges. However, the optimization of the plasma structure should be ascertained in order to explain the complex physical and chemical features in the complicated media having different discharge mechanisms. The non-thermal plasmas are famous especially for the microelectronic systems and surface processes such as etching and purification.

Keywords: *Cold plasma, Gas discharges, Infrared detectors, InGaAs/InP detector*

Cite this paper as: Yücel (Kurt), H.H., & Utaş, S., The features of the InGaAs/InP detectors in plasma converter systems. *Journal of Energy Systems 2022; 6*(4): 534-542, DOI: 10.30521/jes.1105215

1. INTRODUCTION

Recently, with the development of nanotechnology, the interest in plasma technology has increased proportionally [1-3]. Infrared image and visual generating systems prefer the plasma environment. Infrared radiation detection is indispensable tool for device physics and image technology. Unique designed Infrared device structures with doping control of the detector promise significant technological advances such as higher sensitivity cooled Infrared focal plane arrays. New infrared sensor technology needs to be improved for the signal processes [1-3]. The infrared-related studies focused on the infrared avalanche photodiodes. In those systems, a high resistivity semiconductor electrode is used as the infrared detector operating in the near-infrared region. This basic converter system has crucial importance by good sensitivity and high speed of operation [4]. The InGaAs/InP detector is sensitive up to 1700 nm. It can operate in the near-infrared range. It is especially used for the space applications.

InGaAs–InP detectors are specifically designed for single-photon detection [5]. The infrared detectors detect the infrared radiation, when an infrared beam hits the sensor and even they can behave as proximity sensors and have applications in robotic studies. The photon detection efficiency is significantly related to the performance of the detector and InGaAs/InP has good absorption efficiency as a single-photon detector. In that manner, InGaAs–InP single-photon detectors can be evaluated as the most sensitive tools for the weak light detection [1-5]. Indium Gallium Arsenide (InGaAs) (alternatively Gallium Indium Arsenide, GaInAs) is a ternary alloy. The key importance of GaInAs is its application as a high-speed, high-sensitivity photodetector of choice for fiber optic telecommunications [6]. The best visualization method for rendering images in the infrared field is the use of the plasma environment. An infrared radiation detection is an indispensable tool for device physics and image technology. The Infraredworks have focused on infrared avalanche photodiodes. In these systems, a high resistance semiconductor electrode is used as an infrared detector operating in the near-infrared region. This basic transducer system is of crucial importance with good precision and high operating speed [4].

Pearsall invented GaInAs photodiodes in 1977 [7]. InGaAs semiconductor photodetectors can operate at different wavelengths in the laser environment, which is a beam of light. The devices designed for different tasks, which send and receive data at wavelengths of 905 nm, 980 nm, 1060 nm and 1300 nm, have been developed by utilizing technology. InGaAs is used in every field from small devices such as WiFi to large devices such as radar systems, satellites, communication, optics applications and fiber internet line. InGaAs also provides broad gain spectrum and quantum efficiency in quantum well operations. [8]. It is used in a wide variety of fields by adjusting the wavelength with the properties of the different elements it contains [9].

We should consider some parameters to choosing a material as an infrared detector as follows: Spectral response, responsivity, quantum efficiency, and so on. The main part of the Infrared image converters is the micro discharge cell that was found in 1970 [10]. If the wavelength of the incident radiation is greater than λ_{max}, the absorption of the semiconductor material will decrease. This material has gained attention for its applications in LEDs and diodes and detectors in the Infrared region. There has been two important electron emission process in the plasma. Primary avalanche causes the primary electrons and secondary electron emissions are generated by positive ions from the walls and cathode. Secondary electrons have enough energy to start the ionization in the plasma and discharge confinement occurs at only a higher gap distance *d*.

Plasma is electrically neutral to the external environment. That is, the number of positive charges in the plasma is equal to the number of negative charges. Decomposition, ionization, and reconstruction (recombination) events, which are the opposite of these events, occur constantly in the plasma. These events are in a dynamic equilibrium in the plasma among themselves. Plasma is a good conductor of electricity and heat. Experiments clearly show that discharge in the air environment exhibits very

different properties. In some circumstances, unstable situations have also been identified. However, it is extremely important to detect such instabilities to realize the stable and controllable operation of the system at atmospheric pressures.

2. SIMULATION DATABASES AND MEASUREMENTS

2.1. Geometry

The geometric design of the plasma cell is shown in Fig. 1. Here, the distance between the anode-cathode is added to the program as 100 μm. Both the anode and the cathode circumference are divided into regions of certain sizes. SnO_2 material around the anode and InGaAs/InP materials were added around the cathode regions. The design is handled in the 2D asymmetric system due to the easy solving of the program and the plasma cell structure.

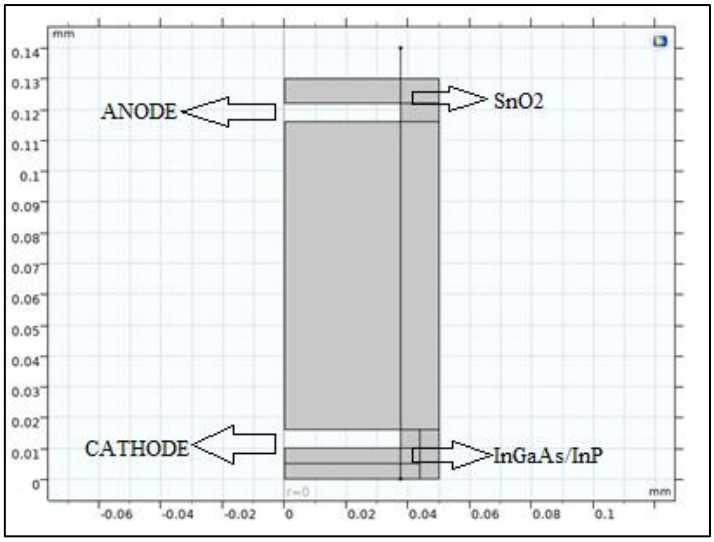

Figure. 1. Plasma cell geometric structure with d=100 μm anode-cathode distance.

2.2. Plasma Chemistry

According to the defined gas, all reaction stages have been shown in Table 1. From the table, we can see that successive Argon ionizations with elastic and inelastic collisions occur and the change of the Townsend coefficient depending on its average energy depends on the change of energy of each electron in the multiplication process [11]. In this region, the grounding values are required for our system. These are the anode, cathode parts, and walls of the plasma system, electrical potential values, and insulating parts, which are identified in the system. The reactions include excitation, ionization, dissociation, recombination, attachment, and detachment, charge transfer, ion recombination, and reactions between neutrals [12].

Table 1. Table of collisions and reactions modeled.

Reaction	Formula	Type	Δε (Ev)	Intensity Constant
1	$e + Ar \longrightarrow e + Ar$	Elastic	0	Boltzmann
2	$e + Ar \longrightarrow 2e + Ar+$	Direct ionization	15.824	Boltzmann
3	$e + Ar \longleftrightarrow e + Ar^{*}$	Excitation	11.424	Boltzmann
4	$e + Ar \longleftrightarrow e + Ar$	Excitation	13.1	Boltzmann
5	$e + Ar* \longrightarrow 2e + Ar+$	Stepwise ionization	4.3997	Boltzmann
6	$2Ar* \longrightarrow e + Ar+ + Ar$	Penning ionization	-	$6.2\times10\text{-}10\ cm^3s^{-1}$
7	$Ar* \longrightarrow hv + Ar$	Radiation	-	$1.0\times107s^{-1}$

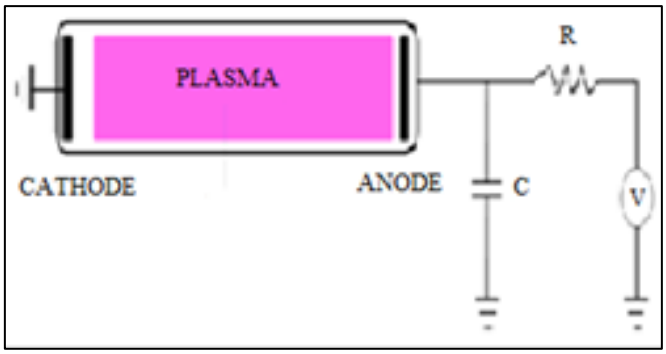

Figure. 2. The DC circuit and components used in the simulation.

According to Fig. 2, resistance-capacitor and voltage source are observed in the plasma system, operated by dc power. By keeping the resistance-capacitor-voltage values fixed, it is possible to observe the formation of plasma through the pressure change.

2.2.1. Field equations

With the drift diffusion equation, we can reach solutions of electron density and mean electron distribution [8, 9, 10, 11, 12].

$$\frac{\partial}{\partial t}(n_e) + \nabla[\, n_e(\mu_e E) - D_e \nabla n_e] = R_e \quad (1)$$

$$\frac{\partial}{\partial t}(n_\varepsilon) + \nabla[- n_\varepsilon(\mu_\varepsilon E) - D_\varepsilon \nabla n_\varepsilon] + E\,\Gamma_\varepsilon = R_\varepsilon \quad (2)$$

$$\Gamma_e = -(\mu_e E)\, n_e - D_e \nabla n_e \quad (3)$$

The electron source R_e and the energy loss due to inelastic collisions R_ε are defined later. The electron diffusivity, energy mobility, and energy diffusivity are computed from the electron mobility using;

$$D_e = \mu_e T_e, \quad (4)$$

$$\mu_e = \left(\frac{5}{3}\right)\mu_e \quad (5)$$

$$D_\varepsilon = \mu_\varepsilon T_e \quad (6)$$

(n_e, electron density; μ_e, electron-ion mobility; D_e, electron mobility; E, Electrostatic field created by ambipolar diffusion; R_e, electron source; T_e, electron temperature; Γ_e, electron flux ($1/(m^2 \cdot s)$). n_ε, μ_ε, D_ε shows inelastic collision values.)

2.2.2. Boundary equations

Except for RF discharges, secondary electron emission and discharge formation process are interrelated. When an ion hits the cathode, an electron is emitted with a certain probability from the cathode surface. When these electrons then obtain enough energy to initiate ionization, they are accelerated by a strong electric field that is close to the cathode. Electrons can be lost due to their random movement at a few mean free path distances from the plasma wall and gain momentum due to the secondary emission mechanism, resulting in the following boundary condition. That is electron flux condition [12]:

$$n\,\Gamma_e = \left(\left(\frac{1}{2}\right) v_{e,th}\, n_e\right) - \sum_p \gamma_p(\Gamma_p\, n) \quad (7)$$

and the electron energy flux,

$$n\,\Gamma_\epsilon = \left(\left(\frac{5}{6}\right) v_{e,th}\, n_\epsilon\right) - \sum_p[\epsilon_p\ \gamma_p\,(\Gamma_p\, n)] \quad (8)$$

(N, number of electrons reaching the anode; γp, contribution margins from my potential release to total yield; Γ_p, positive ion flux; M, reaction that contributes to growth; $v_{e,th}$, moving mass velocity)

2.3. Mesh Structure of Plasma System

The designed mesh structure of our system is of high quality. It is the section where the theoretical calculations of the mesh structure are defined as finite element analysis before analysis has been made to give results closer to the experimental data. Since the analysis data is a more accurate approach according to the mesh types, the mesh structure with 42,500 elements has been applied for the solution.

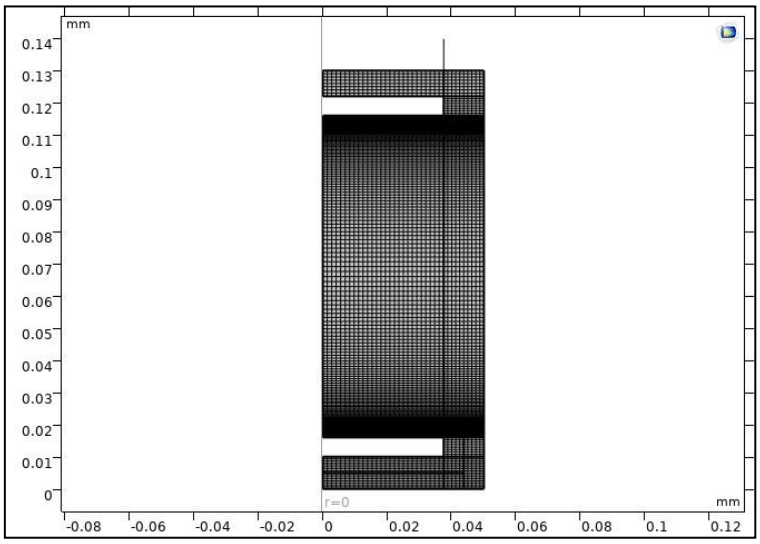

Figure 3. The mesh of the investigated structure.

2.4. Plasma System Theoretical Results

In this section, time-dependent values are put for the formation of the DC discharge zone interval. We have entered the valid and required time values from dc glow discharge to see the plasma formation more easily and to prove the accuracy of the data. Fig. 4 shows current densities forms according to various pressure regimes.

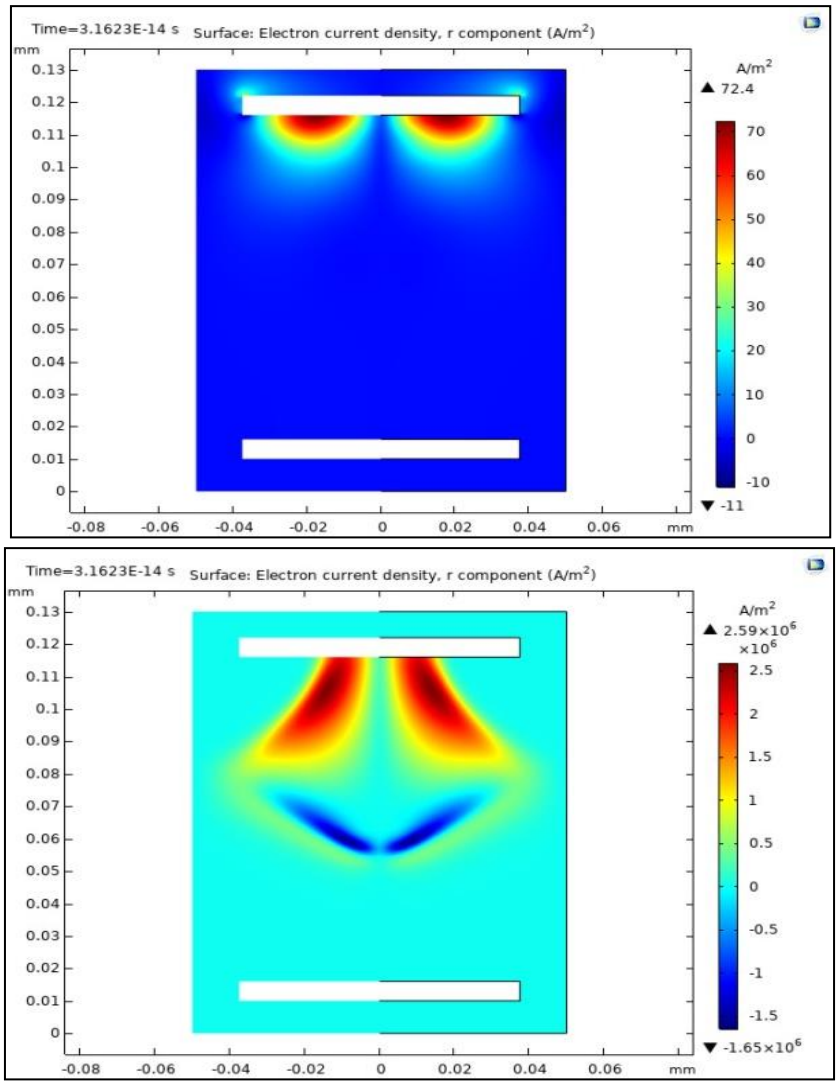

(a)

(b)

Figure 4. Electron Current Densities a) for p=100 Torr, b) for p = 220 Torr.

As can be seen from current density maps, the pressure change made a big influence on the current density values and the current density jumped from the lower (72.4 A/ m^2) to 2.59x10^6 (A/ m^2).

New studies for the stability of plasma brought with it an understanding of the physical and chemical stages of plasma. In anode-cathode system microdischarge cells containing semiconductor, plasma optimization is provided and non-heterogeneous plasma is desired [9, 10, 11, 12, 13, 14].

When the current density is increased beyond 10^{-5} to 10^{-4} A/ cm^{-2}, Townsend discharge turns into Glow discharge [13]. Now, space charge fields play an important role and, the voltage required to sustain the discharge decreases. Positive charge fields and high electric fields formed next to the cathode with cathode drop regions. A positive column of semi-neutral plasma connects the cathode region to the anode region [12].

Fig. 5 shows average mean electron energy values for 220 Torr and 300 Torr.

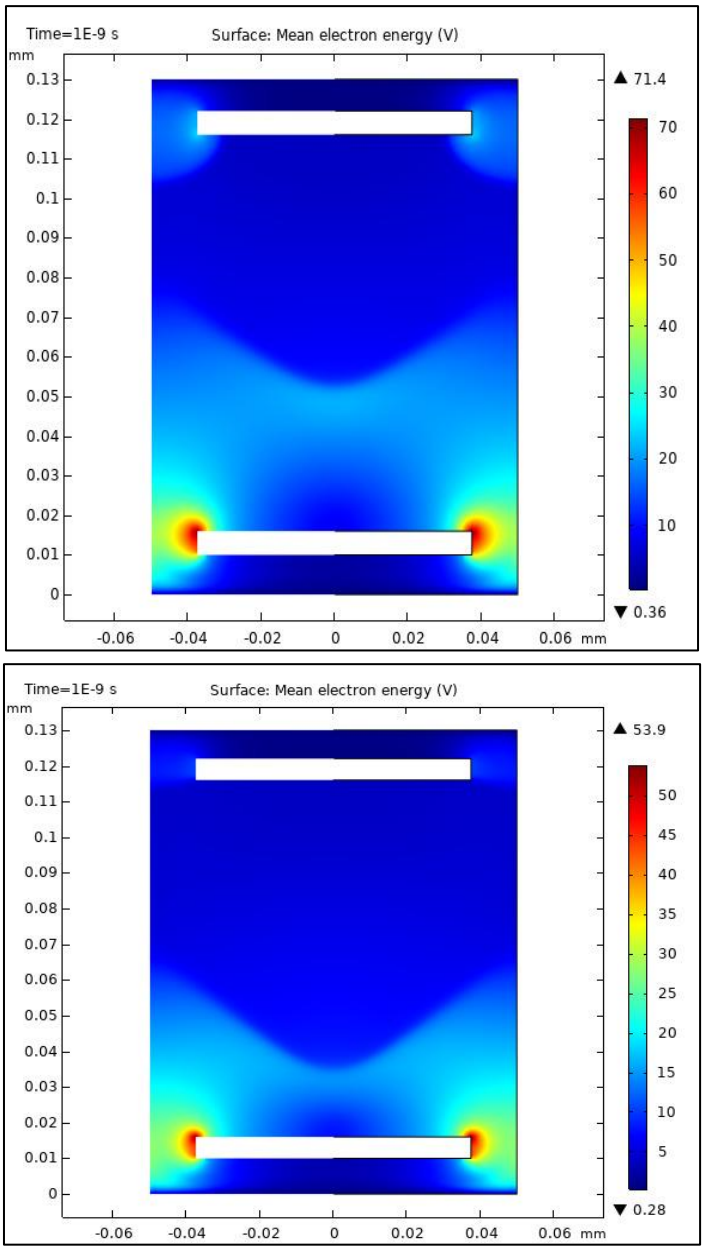

Figure 5. Surface mean electron energy maps: a) for 220 Torr, b) for 300 Torr.

The energy distribution created by electrons is very important in the formation of plasma. Because, it is essential for electron collision reactions. In addition, the electron transport process can be related to this distribution. Electrons have different energies in the plasma. Different plasma chemical process takes a role in a plasma device and each of them is strongly related to electron energy distribution [16,17]. The average energy distribution of the electrons in plasma depends on the electric field which sustains the plasma [15].

We note that the mean electron energy has a higher value for 220 Torr. That is, the secondary electrons gained higher energy for 220 Torr.

In the graphs in Fig. 6, the migrating electron distribution is visualized for 100 and 760 Torr (1 atm). As we approach atmospheric pressure (about 760 Torr), we see that ideal formations (with operation in the flare region) are formed, where the migrating electron flux fields are significantly affected by the current density in the plasma and the hot electrons (red areas in the graphs).

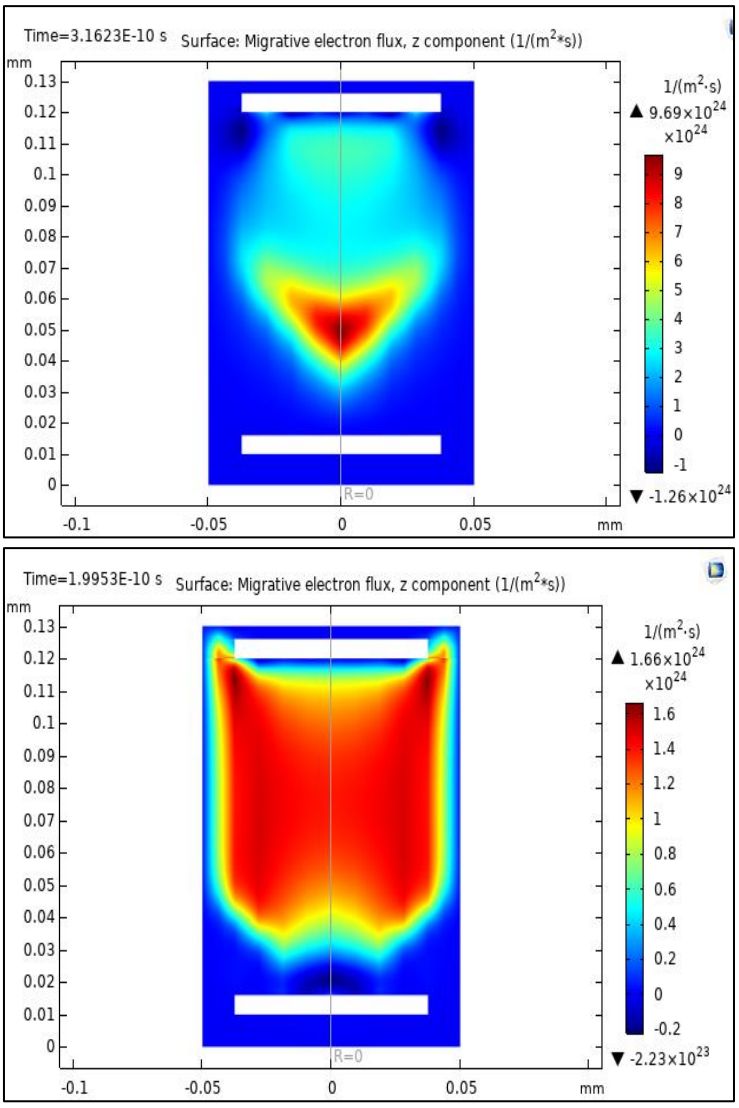

Figure 6. Migrative electron flux maps: a) for 100 Torr b) for 760 Torr.

Electron migration through the cell is the phenomenon that occurs when the semiconductor atoms are under influence of high temperatures and electric current density because of elastic collisions where the electrons transfer their momentums to crystal in the direction of electron propagation. The ion mobility is much lower than electron mobility in plasma. Therefore, the plasma formation and electric field movements are generally governed by electron migration flux [16, 17, 18].

3. CONCLUSION

The COMSOL simulation program was used at different operating pressures to show the available density maps. The two-dimensional (2D) electron migration flux is analyzed by COMSOL in a uniform electric field. If the voltage applied between the electrodes (anode and cathode) is increased enough, the current will reach saturation. If the applied voltage is further increased, the current will increase exponentially and the electrons will have enough energy to ionize a neutral atom. Thus, the breakdown breakdown voltage, electron speeds, and glow zone conditions, which are the ideal plasma operating range, were determined for plasma formation. The increase in working pressure also showed variability in the data analyzed in the graphs.

Heterostructures and devices are grown commercially, and these composite structures have strong absorption in emission energy for device applications [16, 17, 18]. To verify the efficacy of binary compound materials for the plasma transport mechanism, the InGaAs/InP detector is chosen as a cathode material. As a result of different pressures, we investigated InGaAs/InP composite cathode materials and plasma system performance for optimization of future device applications [17, 18]. In the following years, plasma systems can be developed and orientation to different areas can be realized. In recent years, the importance of tokamak and fusion energies, the importance of detector materials and the requirement of unlimited energy needs have directed those who work on this subject to single and compound materials in different structures.

REFERENCES

[1] Fang, YQ, Chen, W, Ao, TH, Liu, C, Wang, L., Gao, XJ, ... & Pan, JW. InGaAs/InP single-photon detectors with 60% detection efficiency at 1550 nm. *Review of Scientific Instruments* 2020*;*, *91*(8): 083102. https://doi.org/10.1063/5.0014123

[2] Tatsuoka, H, Kuwabara, H, Nakanishi, Y, Fujiyasu, H. Growth of CdTe(111)B homoepitaxial layers by hot-wall epitaxy. *J. Appl. Phys*. 1991; *69*: 6472-6477.

[3] Eisaman, MD, Fan, J, Migdall, A, Polyakov, SV. Invited review article: Single-photon sources and detectors. *Review of scientific instruments* 2011; *82*(7): 071101.

[4] Rogalski, A. *Infrared and Terahertz Detectors*. CRC Press., 2019.

[5] A. F. Holleman, E. Wiberg and N. Wiberg, W. Holleman, Lehrbuch der Anorganischen Chemie, chap. Die Zinkgruppe, 101 edn. de Gruyter, Berlin – New York, 1995, pp. 1375

[6] Toprak, MA. Electronic energy spectrum of GaAs/InxGa1-xAs quantum wells. MSc, Cunhuriyet University, Sivas, Turkiye, 2013.

[7] Kish, F, Lal, V, Evans, P, Corzine, SW, Ziari, M, Butrie, T, Welch, D. System-on-chip photonic integrated circuits. *IEEE Journal of Selected Topics in Quantum Electronics* 2017; *24*(1): 1-20.

[8] Bimberg, D., Kirstaedter, N., Ledentsov, N. N., Alferov, Z. I., Kop'Ev, P. S., & Ustinov, V. M. (1997). InGaAs-GaAs quantum-dot lasers. *IEEE Journal of selected topics in quantum electronics*, *3*(2), 196-205.

[9] Temkin, H., Alavi, K., Wagner, W. R., Pearsall, T. P., & Cho, A. Y. (1983). 1.5–1.6-μm Ga0. 47In0. 53As/Al0. 48In0. 52As multiquantum well lasers grown by molecular beam epitaxy. *Applied physics letters*, *42*(10), 845-847.

[10] Kasymov, SS, Paritskii, G. Device for tracking images. *Russian Authors' Certificate* 1973; *1798020*: 18-10.

[11] Sakiyama, Y, Graves, DB, Chang, HW, Shimizu, T, Morfill, GE. Plasma chemistry model of surface Micro discharge in humid air and dynamics of reactive neutral species. *J. Phys. D: Appl. Phys*. 2012*; 45*: 425201

[12] Rafatov, I, Bogdanov, EA, Kudryavtsev, AA. On the accuracy and reliability of different fluid models of the direct current glow discharge. *Phys.Plasmas* 2012; *19*(3): 033502.

[13] Yu, A, Astrov, A.N. Lodygin, and Portsel, LM, Townsend discharge in nitrogen at low temperatures: enhanced noise and instability due to electrode phenomena. *J. Phys. D Appl. Phys*.2016; *49*: 2016: 095202.

[14] Ikhmayies, SJ, Kurt, HH. (Eds.). (2021). *Advances in Optoelectronic Materials*. Springer International Publishing. https://doi.org/10.1007/978-3-030-57737-7

[15] Godyak, V. A. Electron energy distribution function control in gas discharge plasmas. *Physics of Plasmas* 2013; *20*(10): 101611.

[16] Kurt, H.H., Tanrıverdi, E., Electrical properties of ZnS and ZnSe semiconductors in a plasma-semiconductor System. *Journal of Electronic Materials* 2017; *46*(7): 3965-3975

[17] Kurt, H.H., Tanrıverdi, E. The Features of GaAs and GaP Semiconductor Cathodes in an Infrared Converter System. *Journal of Electronic Materials* 2017; *46*(7): 4024-4033.

[18] Sadiq, Y., Kurt, H.Y., Albarzanji, A.O., Alekperov, S.D., Salamov, BG. Transport properties in semiconductor-gas discharge electronic devices. *Solid-state electronics* 2010; *53*(9): 1009-1015